INSTITUTE OF SPACE AND ASTRONAUTICAL SCIENCE
YOSHINODAI, CHUO, SAGAMIHARA, KANAGAWA 252-5210

ISAS RESEARCH NOTE

ISAS RN 864

Effects of Plasma Generated by Hypervelocity Impact on Planar Structure

Yoichi NAGAOKA [1], Koji TANAKA [2], Susumu SASAKI [2]

January 2012

1 : The Graduate University for Advanced Studies
2 : Institute of Space and Astronautical Science,
Japan Aerospace Exploration Agency

Effects of Plasma Generated by Hyper-velocity Impact on Planar Structure

Yoichi NAGAOKA, Koji TANAKA and Susumu SASAKI

Key Words: Spacecraft, Hyper-velocity Impact, Plasma Propagation, Charging

Abstract: We have carried out hyper-velocity impact experiments on planar targets using a two-stage light gas gun, to study propagation and charging effect of the impact plasma associated with an interference with solar array in space. Propagation of the luminous cloud and generated plasma were observed by a high-speed video camera and an array of plasma probes, respectively. It was found there existed a high density plasma propagating along the surface of the plate at a high-speed more than the projectile velocity. The electric potential of the target increased up to 10 V at the impact. The characteristic behaviors of the plasma propagation and potential electric change were explained by the half-range Maxwellian plasma ejected from the collision area.

1. Introduction

The solar array panel is usually the largest part of spacecraft exposed to the space environment. For example, a 10 kW spacecraft power system requires a solar panel area more than 30 m^2. The solar array panels in many occasions are susceptible to hyper-velocity impact by space debris or meteoroid more than 1 mm size during the mission life. The hyper-velocity impact gives four types of damages to the solar array panel as shown in Fig.1. Piercing through or penetration destroys the cell at the impact point, but the mechanical damage is generally localized at the target cell. Back-scattered fragments or vapor contaminate the surface of the cells and degrade the optical performance of the cell, but they are also localized near the impact point. On the other hand, the impact plasma generated at the impact can give an electrical effect in a wider area surrounding the collision point. The impact plasma could induce electrical discharge at the cells or interconnections especially if they are operated at high voltages more than 100 V. Currently the solar array voltage for standard satellites is mostly less than 60 V, but for higher power satellites at a 10 kW level, a bus voltage more than 100 V will be used to reduce the power losses in the power system. Actually, 160 V solar array voltage is used for the International Space Station. As another effect of the impact plasma generation, the potential of the pane can be changed or fluctuated, just like the case in the plasma production by a pulsed laser irradiation. The potential change will propagate the wires in the solar array panel and may give a harmful interference in the power systems.

In the past hyper-velocity impact experiments on the solar cell coupon panels[1,2], the critical voltage for the cell discharge and types of the discharge have been investigated. Very few has been reported on the behaviors of impact plasma that causes the electrical interferences with the solar array cells. From a view of pulsed plasma generation, the impact-generated plasma has a certain similarity with the laser-generated plasma[3.4], but the features of plasma propagation are quite different, because the laser plasma propagates in a hemisphere from a fixed irradiation point while the impact plasma propagates under a restriction of geometry of the projectile penetrating into the target. Also in the case of impact plasma, the locations of the plasma production and plasma ejection change with time during the penetration.

The objectives of our experiment are to clarify the behavior of the impact plasma using plasma probes distributed near the target and to evaluate the charging effect of the target at the plasma production. In our impact experiment, we use a spherical metal projectile and planar metal target, rather than the actual solar cell consisting of multi-layer materials, to study the plasma propagation in a simple configuration with one or two plasma components. Once the plasma propagation model is established, it will be possible to predict quantitatively the plasma environment near the surface of spacecraft impacted by the space debris

or meteoroid, and to assess the possible risk for spacecraft.

2. Experiments

The hyper-velocity impact experiment was conducted by a two-stage light gas gun at the Institute of Space and Astronautical Science, JAXA. This system can accelerate a metal sphere projectile of several tens of milli-gram up to 6 km/s. Figure 2 shows the experimental setup consisting of the gas gun and an impact chamber in which the planar target and plasma probes were installed. Figure 3 shows the inside configuration of the impact chamber. Totally 14 plasma probes were distributed near the target; 10 probes in the front side (impact side) and 4 probes in the rear side. The angle θ referred here is measured from the normal line of the target. The distance of each probe from the impact point in the front side was 60 mm at θ = 30 °, 45 °, 60 ° and 75 °, and was distributed between 100 mm and 200 mm at θ = 90 ° (along the target surface). In the rear side, the probes were distributed from 40 mm to 140 mm from the impact point. The plasma probe we used was the double probe consisting of two disk-electrodes 6 mm in diameter, separated at a distance of 10 mm. The bias voltage between the electrodes was fixed at 10 V.

Besides the plasma measurement, we observed the luminous emission from the impact-generated cloud using a high-speed video camera and photo-diodes with optical filters. The images were taken every two μs, which gives two dimensional information of luminous cloud motion. The three photo-diodes filtered at 500 nm, 700 nm, and 900 nm with a bandwidth of 40 nm gives the information of the luminous gas temperature under the black-body approximation.

We used an Al projectile, spherical 3.2 mm in diameter and 50 mg in weight. The impact velocity was between 5.5 km/s and 6 km/s. For the impact target, we used 5 kinds of metal plate; Al, Ti, Cu, Ag, and Ta with 100 - 500 μm in thickness. The experiments were carried out in a vacuum less than 4×10^{-2} Pa, to avoid the collisional effect of the residual gas to the plasma propagation. This pressure range corresponds to the mean free path of air longer than 200 mm.

Figure 4 is the configuration for electrical potential measurement. Figure 5 is the equivalent circuit for electrical potential measurement.

3. Experimental Results

A typical example of the probe current measured by the double probes, Ch4, 5 and 6, is shown in Fig.6 when the projectile was impacted to an Al target of 300 μm thick at 5.5 km/s – 6.0 km/s. The probe current is proportional to the plasma density if the electron temperature is assumed to be the same. Using the current data measured by each probe, we obtained the spatial distribution of the density and propagation velocity of the impact plasma. Figure 7 shows a typical example for a series of images of the luminous cloud when the projectile was impacted to an Al target of 300 μm thick at 5.5 km/s – 6.0 km/s. By tracking the edge of the cloud, we can obtain the propagation speed of the cloud in two dimension. The edge velocity after 6 μsec is seemingly decreased, which could be caused by the intensity reduction with the expansion of the cloud gas. The past experiments suggest the luminous emission at the impact is radiated mainly from the hot neutral gas. The gas temperature was obtained from the light intensities in the three bands by assuming the black-body radiation process. The temperature was analyzed to be approximately 5000 °K – 10000 °K at the impact.

We have obtained the plasma density from the probe current for the range of electron temperature from 5000 °K to 10000 °K, by assuming the local thermal equilibrium for the gas and plasma at the impact. Since we have no information on the species of plasma ion, we use the atomic mass both for the projectile (aluminum) and the target in the calculation. The maximum plasma density derived from the maximum current is shown in Fig.8a. The error bar means the divergence by the temperature range from 5000 °K to 10000 °K and also by the mass range for the projectile and target. In order to obtain the dependence of the

plasma density on the distance from the impact point, the plasma density and distance for each data set are normalized by those for the nearest probe as shown in Fig.8b. There is a tendency that the plasma density is decreased as the minus 3rd power of the distance near the impact point as shown by broken line, but it is decreased more rapidly in the longer distance. This can be explained by the effect of the ambient gas density near the target at the impact. Before the impact, the ambient gas was well evacuated so as that the plasma particles did not collide with the background gas molecules during the propagation more than 200 mm. However, a PET film installed between the gas gun and the impact chamber was partially evaporated when the projectile went through the PET film and the generated gas reached the surface of the target. The pressure at the impact was not measured in our experiment, but the dependence of the plasma density on the distance can be explained if we assume the ambient pressure increased from 0.01 Pa to 0.1 Pa.

Figure 9 shows the dependence of the plasma density on the propagation angle for the Al target in the thickness range from 100 μm to 500 μm. The plasma density at 10 cm from the impact point was calculated from the probe data at different distances using the experimental dependence shown in Fig.8b. The plasma propagated mostly at the angle beyond 60 ° (near the target surface). The experimental results show that a high-density plasma, $10^{13\sim14}$ cm^{-3} at 10 cm from the impact point, propagated along the surface of the target, which could strongly interact with the solar cells if they had been on the plate.

Figure 10 shows the dependence of the propagation velocity on the propagation angle. The propagation speed is calculated for the peak of the probe. Since the probe signals below 60 ° are too small to identify the timing of the peak, the data more than 60° are only used for the analysis. The propagation velocity gets higher as the propagation angle approaches 90 ° (along surface of the target). For comparison, the propagation velocity derived of the edge of the luminous cloud was calculated from the series of the images from the high-speed video camera. Considering the reduction of the light intensity for the propagating the luminous cloud, images before 4 μsec are used for the calculation. The propagation velocity for the plasma and the luminous cloud has nearly the same profile, which means they are in local thermal equilibrium at the initial phase when they are produced by the impact. Figure 11 shows the dependence of the propagation velocity on the propagation angle.

Most of the impact experiments were conducted for the target grounded to the conductive chamber wall. However, in order to study the charging effect of the plasma production to the target, we made the impact experiment to the target electrically isolated from the chamber wall several times. In the experiment, the capacitance between the target and the chamber wall was adjusted as 500 pF. Figure 12 shows the typical result when the Al target was impacted at the velocity of 5.5 km/s. The initial voltage reached 10 V within 50 ns and then decreased slowly with time. It is interpreted that the electrons faster than the ions caused the rapid initial positive charging and then the charging was relaxed in the effect of the macroscopic plasma motion in the target chamber.

4. Discussions

4－1. Plasma probe measurement

The jetting model[5] based on the shock wave theories has been proposed for the ejectors at the hyper-velocity impact. When two plates are collided obliquely, a mass and momentum flow is generated under certain conditions. The theory has been verified experimentally by the symmetric oblique collision of thin plates. For our case in which a sphere collides with a plate, the collision angle changes with time. It has been theoretically predicted that the jet is formed when the collision angle exceeds a critical angle. Actually the mass flow observed in the sphere-plate collision has been explained by the jetting theory in many experiments. However, there is no report on the existence of the critical angle for the propagation of impact plasma. In our experiment, we have observed the plasma propagating along the target surface and detected no critical angle for the propagation. Here we discuss a plasma propagation model to explain our experimental results.

In our model, we assume that the hot gas partially ionized is generated at the overlapping area between the projectile and the target, and is transported to the edge of the collision area, and is ejected to the open space, as shown in Fig.13. In the model calculation, we have following specific assumptions;

1. The material in the overlapping area of the projectile and the target is heated, fragmented, vaporized, and released as ejectors. The ionization degree in the ejection mass flow is constant throughout the collision process.
2. The plasma is ejected uniformly to the open space in the angle between the projectile and target.
3. The velocity distribution of the plasma is single-Maxwellian.
4. The plasma temperature is the same as the gas temperature in the range of 5000 – 10000 °K observed in the experiment.
5. The species of the plasma ion is single, which is the case of Al-Al collision in our experiments.

Based on the assumptions, the plasma production rate Q(t) is expressed as,

$$0 \le t \le t_1 \qquad Q(t) \propto 2\pi\rho v_0\{{r_0}^2 - (r_0 - v_0 t)^2\} \qquad (1)$$

$$t_1 \le t \le t_2 \qquad Q(t) \propto 2\pi\rho v_0 d\{2(r_0 - v_0 t) + d\} \qquad (2)$$

Here, t_1 ($t = d/v_0$) is the timing when the front of the projectile reaches the rear side of the planar target, and t_2 is the timing when the projectile gets through the target. The plasma production rate is maximum at $t = t_1$, as is expressed;

$$Q_{max} \propto 2\pi\rho v_0 d(2r_0 - d) \qquad (3)$$

The solid angle in which the plasma can propagate is;

$$\Omega = \frac{2\pi\sqrt{{r_0}^2 - (r_0 - v_0 t)^2}}{r_0} = 2\pi\cos\theta \qquad (4)$$

The plasma ejection rate per unit solid angle is expressed by the collision angle θ between the normal line of the target and tangential line of the projectile sphere as;

$$\theta_1 \le \theta \le 90 \qquad q(\theta) \propto \rho v_0 {r_0}^2\cos\theta \qquad (5)$$

$$\theta_2 \le \theta \le \theta_1 \qquad q(\theta) \propto \frac{\rho v_0 d(2r_0\sin\theta + d)}{\cos\theta} \qquad (6)$$

here,

$$\theta_1 = \cos^{-1}\left(\frac{\sqrt{{r_0}^2 - (r_0 - d)^2}}{r_0}\right) \qquad (7)$$

$$\theta_2 = \sin^{-1}\left(-\frac{d}{2r_0}\right) \qquad (8)$$

θ_1 ($t = t_1$) is the angle when the projectile reaches the rear side of the planar target, and θ_2 ($t = t_2$) is the angle when the projectile gets through the target. Figure 14 shows the dependence of the plasma ejection rate on the collision angle θ. The ejection rate increases as θ decreases from 90 ° and reaches a maximum at $\theta = \theta_1$, and then decreases as θ approaches θ_2. The plasma ejection rate to the front side is reduced more than the calculation when $\theta < \theta_1$, because the generated plasma is ejected to the rear side as well.

The plasma ejection point moves with time as shown in Fig.13. The velocity v_{eject} is expressed as;

$$v_{eject} = \frac{v_0(r_0 - v_0 t)}{\sqrt{r_0^2 - (r_0 - v_0 t)^2}} = v_0\tan\theta \qquad (9)$$

The velocity v_{eject} can be higher than the velocity of the projectile when θ is larger than 45 °. Especially, it gets extremely high near θ = 90 ° along the target surface. The plasma ejection velocity is biased by the drift velocity v_d, which is the radial component of v_{eject}. Then the velocity distribution of the plasma in the laboratory frame is a drift-Maxwellian expressed as;

$$f(v) = \left(\frac{\alpha}{\pi}\right)^{\frac{3}{2}} (v - v_d)^2 \mathrm{e}^{-\alpha(v-v_d)^2} \quad (10)$$

here, $\alpha = m/2k_BT = 1/v_{th}^2$. The plasma density at a distance L from the impact point is obtained as;

$$n(t) = \frac{1}{L^3}\left(\frac{\alpha}{\pi}\right)^{\frac{3}{2}} (v_d + v_x) v_x^2 \mathrm{e}^{-\alpha v_x^2} \quad (11)$$

here, $v_x = L/t - v_d$. The timing of the maximum plasma density is obtained if we set $dn(t)/dt = 0$. This gives a relation as;

$$3v_x - 2\frac{v_x^3}{v_{th}^2} + 2v_d\left(1 - \frac{v_x^2}{v_{th}^2}\right) = 0 \quad (12)$$

Eq.(12) indicates that v_x is between $1.0v_{th}$ and $1.2v_{th}$ regardless of the value of v_{th}. If we consider that the v_x is approximately constant, the maximum plasma density n_{max} is decreased with the distance as L^{-3}.

4-2. Electrical potential

From Eq.(10), we can calculate the number of the electrons N_{escape} escaping from the target which causes the charging of the target up to V_c. By neglecting v_d in Eq.(10) as the electron velocity corresponding to V_c is much larger than v_d, N_{escape} can be expressed in terms of energy as;

$$\frac{CV}{e} = N_{total} \int_V^\infty f(\varepsilon) d\varepsilon \quad (13)$$

Here, N_{total} is the total amount of the plasma production at the impact. In our experiment, the probe measurements indicate N_{total} was typically 10^{16} /cm^{-3}. On the other hand, the charging voltage is expressed from the N_{escape} as:

$$\frac{C}{eN_{total}} = \frac{\int_V^\infty f(\varepsilon) d\varepsilon}{V} \quad (14)$$

Here, C is the capacitance between the target and the chamber wall, and e is the charge of the electron. From Eq.(14), we can obtain the charging voltage as 4 V for T_e = 5000 °K and 7 V for T_e = 10000 °K in our model calculation.

The comparison between the model calculation and experimental results are summarized as follows.

(1) The model based on the drift Maxwellian distribution suggests that the plasma density is deceased with the distance as L^{-3}. The experimental results show that it decreased as L^{-3} near the impact point, but the reduction was more in the longer distance. If we assume that the background gas density was increased up to 0.1Pa, the experimental results are reasonably explained by our model. Since the possible increase of the ambient gas density is peculiar to the laboratory experiment configuration, the L^{-3} dependence is applicable to the impact phenomena in space. The plasma density observed in our experiment was as much as 10^{14} cm^{-3} at 10 cm from the impact point, which is much higher than the ionospheric plasma density by the 8th order of magnitude. If we apply the experimental results directly to the solar array panel in space, the area for the discharge risk[6], plasma density more than 10^{10} cm^{-3}, could be extended 1 - 2 m around the impact point.

(2) In the model, the plasma ejection is limited by the geometry of the projectile and target. The allowable angle for the plasma propagation is limited between 90 ° and θ. θ changes with time from 90 ° to θ_2. On the other hand, the plasma production rate is maximum at $\theta = \theta_1$ as shown in Eq.(3). By assuming that the plasma is propagated uniformly in the allowable angle, the plasma propagation flux per solid angle is maximum at $\theta = \theta_1$ in the angle between 90 ° and θ_1, and at each θ in the angle between θ_1 and θ_2. This model suggests the peak plasma density is maximum in the direction along the target surface and is decreased as separated from the surface. The experimental results show that the plasma density was maximum between 70 ° and 90 ° and decreased as the angle gets smaller. Thus the model can explain the tendency of the experimental results.

(3) Since the model assumes the plasma propagation from the edge of the collision that moves outwards at the velocity v_{eject}, the

velocity of the plasma peak is expressed as $v_x + v_d$ from Eq.(11). Thus the velocity of the plasma peak is maximum at $\theta = 90$ ° and is decreased as the angle decreases, which is consistent with the experimental result. The peak velocity along the target surface is calculated as 17 km/s – 8 km/s for $T_e = 10000$ °K in the range of thickness from 100 μm – 500 μm. The experimental results show the peak velocity along the target was 16 km/s – 12 km/s. The characteristic features of the plasma propagation velocity are explained by the model.

(4) The charging of the target at the impact is explained by the Maxwellian electron energy distribution. According to the model, the charging voltage is calculated as 4 V – 7 V for the total plasma production 10^{16} /cm^{-3} at the impact, which is consistent with the experimental result. If we apply this model to spacecraft with 1000 pF, corresponding to a 10 m diameter sphere in space, the charging is expected to be 5 V for the same plasma production as our experiment. The charging effect could be larger for the larger plasma production.

5. Conclusion

We have made hyper-velocity experiments to thin planar metal of 100 μm -500 μm thickness using an aluminum projectile of 3.2 mm diameter with a velocity of 5.5 km/s - 6.0 km/s, and studied the effects of the impact plasma to the target. It was found that the impact plasma propagates mainly within 30 ° from the target surface and the propagation velocity was maximum along the target surface. The plasma density was found to decrease as the minus 3rd power of the distance if we eliminate the collision effects with the ambient gas molecules. The charging effect of the target by the impact plasma was measured around 10V. These results have been explained by a model in which the impact plasma is ejected uniformly in the allowable open space with an initial velocity distribution of Maxwellian type. In order to apply our model to the impact plasma effects to spacecraft, we need to know the amount of total plasma production at the impact. The amount of the plasma production depends not only on the velocity and mass of the projectile, but also on the material and thickness of the target. By making a database of the plasma production for these parameters, we will be able to predict the impact plasma environment and to evaluate the risk of impact plasma more quantitatively for spacecraft design and failure mode analysis.

Acknowledgement

The research results were obtained using Space Plasma Laboratory of ISAS, JAXA.

References

1) Brandhorst, H. : Hypervelocity Impact Studies of High Voltage Solar Array Segments, 53rd IAC, 2002, IAC-02-R.P.06

2) Crawford, D. A. and Schultz, P. H. : Laboratory Investigations of Impact-generated Plasma, Journal of Geophysical Research, 96 (1991), pp.18807-18817.

3) Krasa, J., Picciotto, A., Gammino, S., Laska, L., Rohlena, K., Torrisi, L. : Time-of-flight spectroscopy of ion currents emitted by laser produced plasmas, 33rd EPS Conference on Plasma Physics, 30I (2006), P-1.030

4) Bleiner, D. and Bogaerts, A. : Laser-induced plasmas from the ablation of metallic targets: The problem of the onset temperature, and insights on the expansion dynamics, Journal of Applied Physics, 101 (2007), pp.083301-1-5.

5) Jean, B. and Rollins, T. L. : Radiation from Hypervelocity Impact generated Plasma, AIAA J., 8 (1970), pp.1742-1748

6) Stevens, N. J. : Summary of PIX-2 Flight Results over the First Orbit, AIAA 24th Aerospace Sciences Meeting, 1986

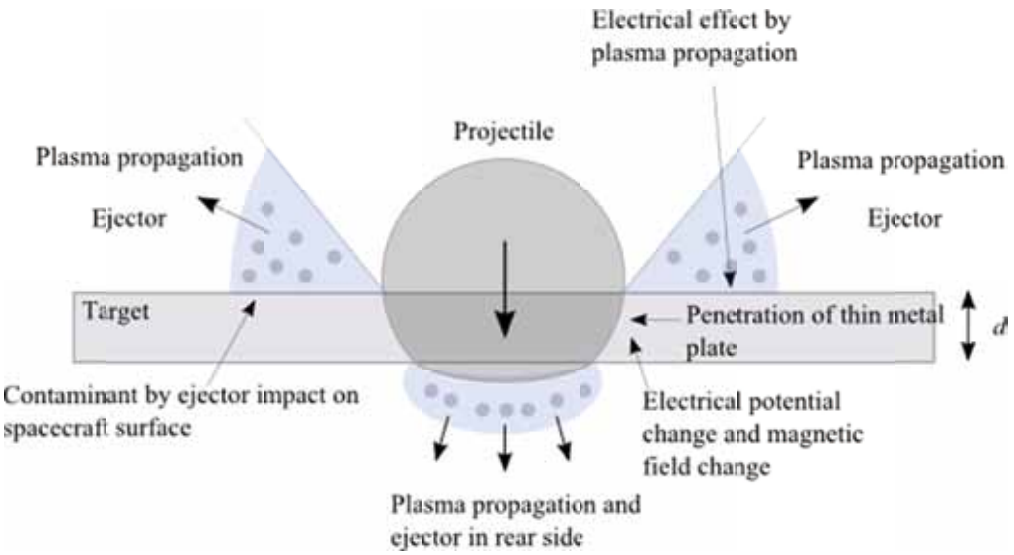

Fig. 1. Electrical effects for impact between spacecraft and space debris.

Fig. 2. Two-stage light gas gun and experimental chamber.

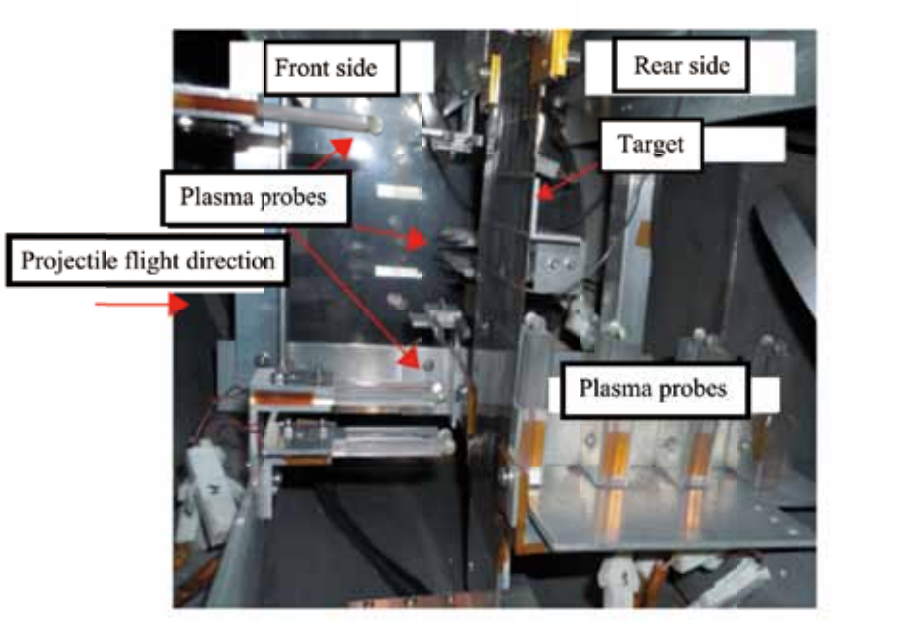

Fig. 3a. Experimental chamber.

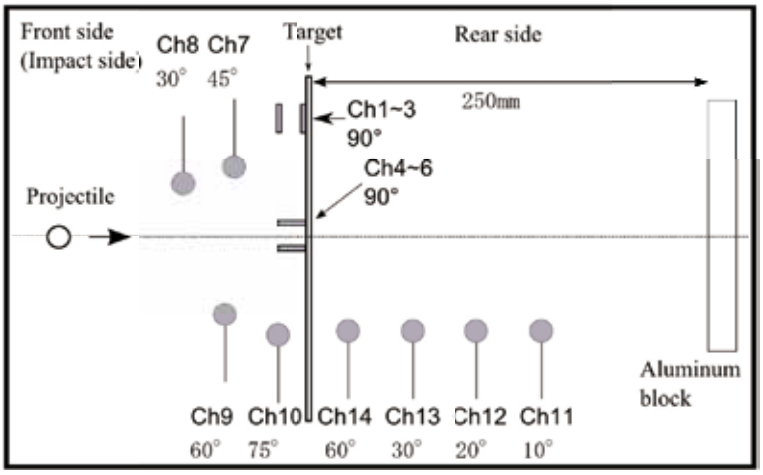

Fig. 3b. Experimental setup for the double probe measurement.

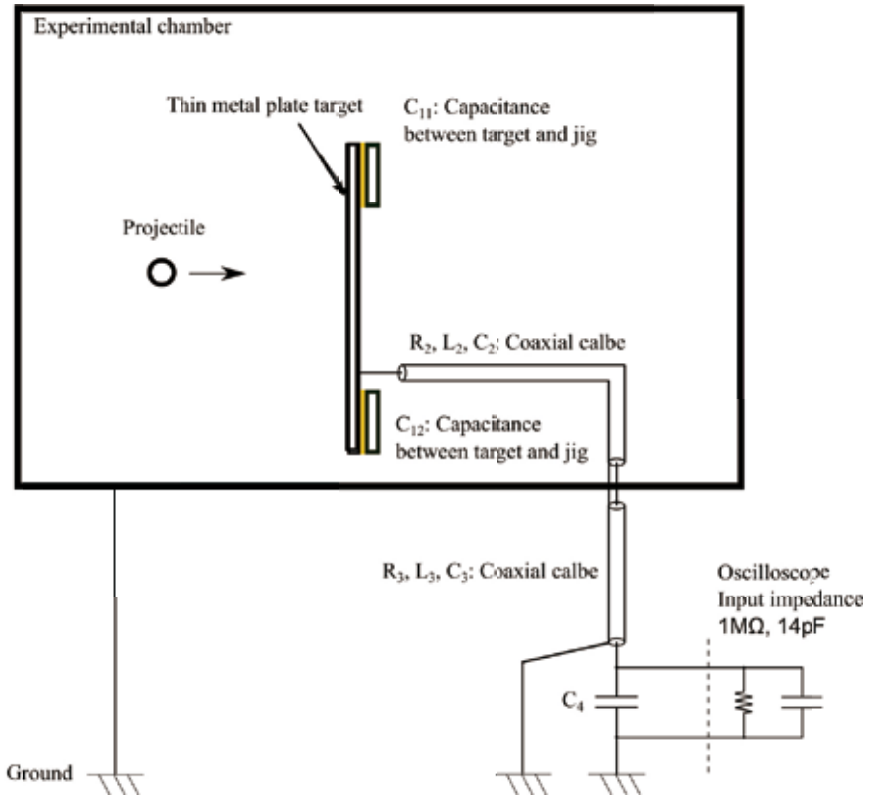

Fig. 4. Experimental setup for electrical potential measurement.

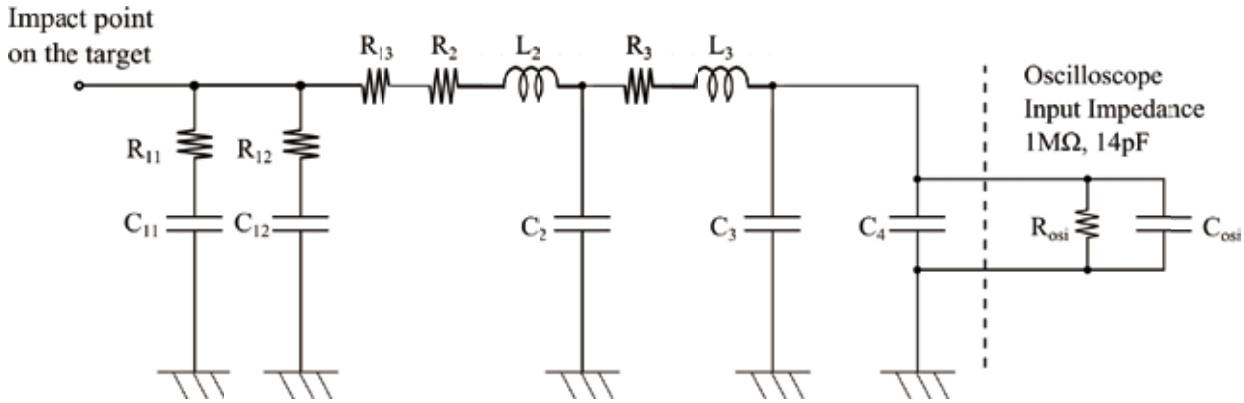

Fig. 5. Equivalent circuit for electrical potential measurement at target.

R_{11}, R_{12}, R_{13} : Resistance from the impact point

C_{11}, C_{12} : Capacitance between target and jig

R_2, L_2, C_2 : Coaxial cable, (0.1Ω/m, 250nH/m, 100pF/m)

R_3, L_3, C_3 : Coaxial cable, (0.1Ω/m, 250nH/m, 100pF/m)

C_4 : Ceramic capacitor, 54.4pF

R_{osi},C_{osi} : Oscilloscope input impedance, (1MΩ, 14pF)

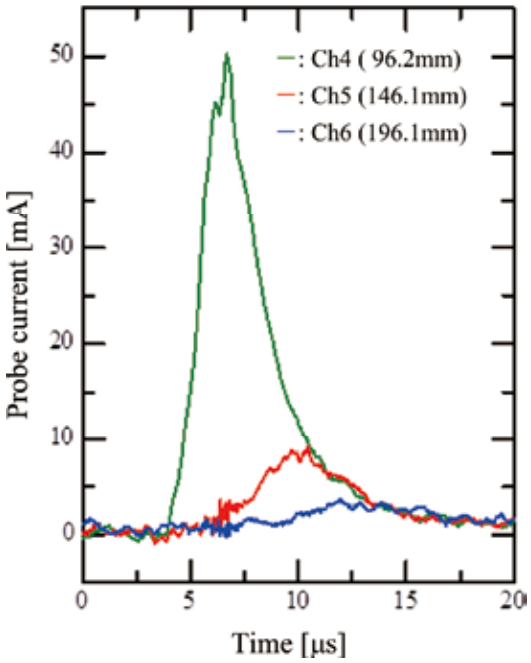

Fig. 6. Plasma probe current waveforms.

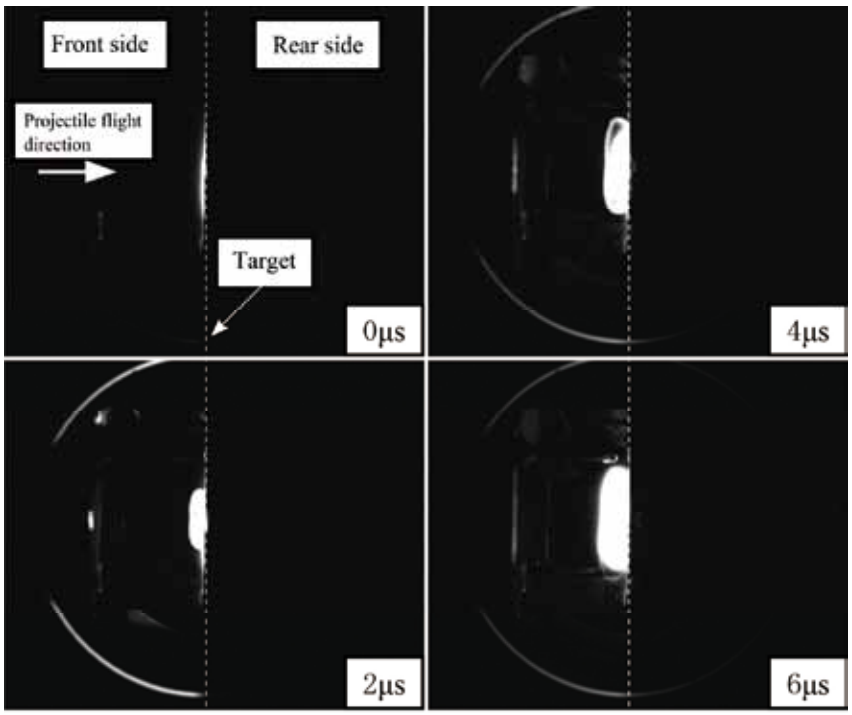

Fig. 7. A series of images by high-speed video camera. Luminous cloud was propagating along the target plate surface of the front side.

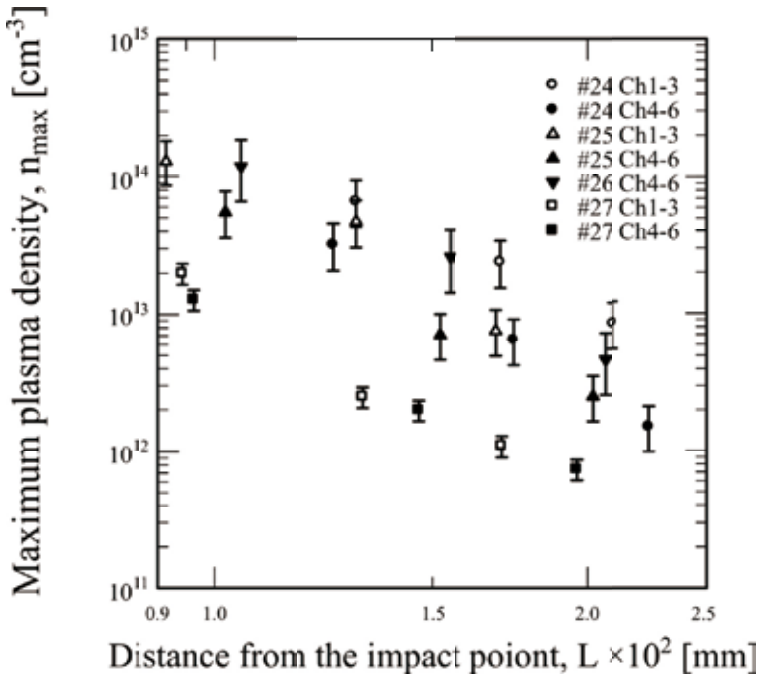

Fig. 8a. Relation of the propagation distance to the maximum Plasma density.

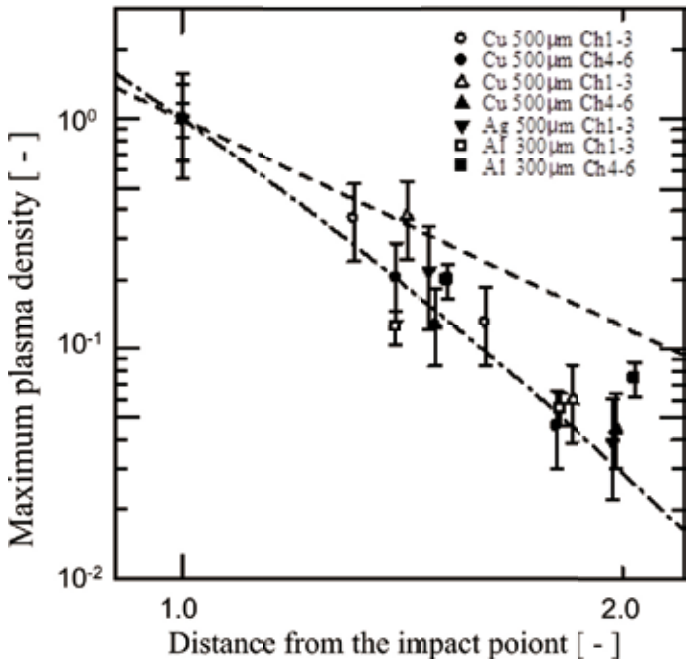

Fig. 8b. Relation of the normalized propagation distance to the normalized maximum Plasma density.

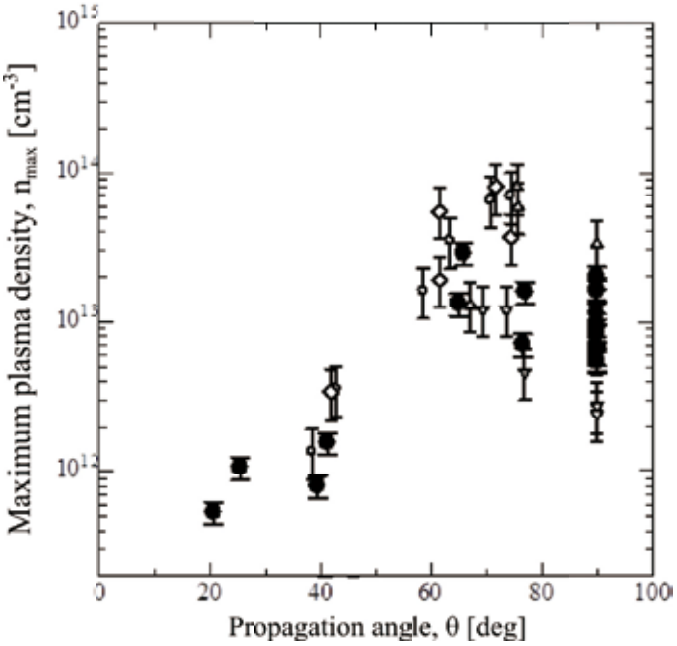

Fig. 9. Relation of the propagation angle to the maximum plasma density.

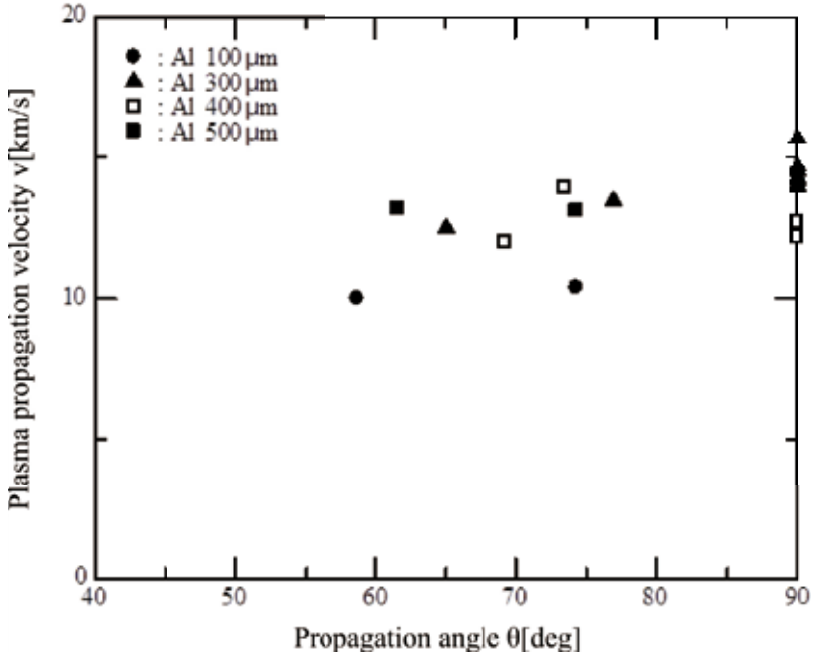

Fig. 10. Relation of the propagation angle to the plasma propagation velocity.

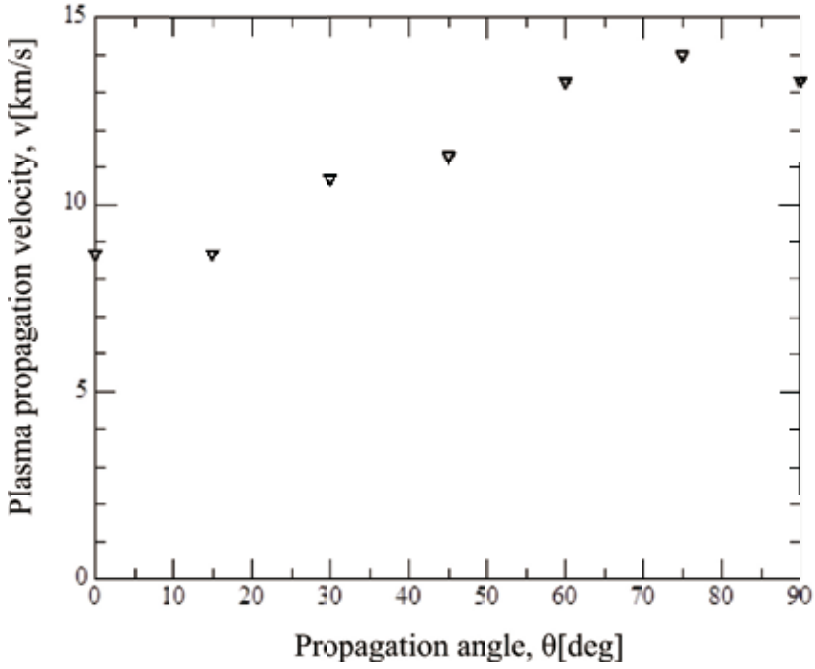

Fig. 11. Relation of the propagation angle to the luminous cloud velocity.

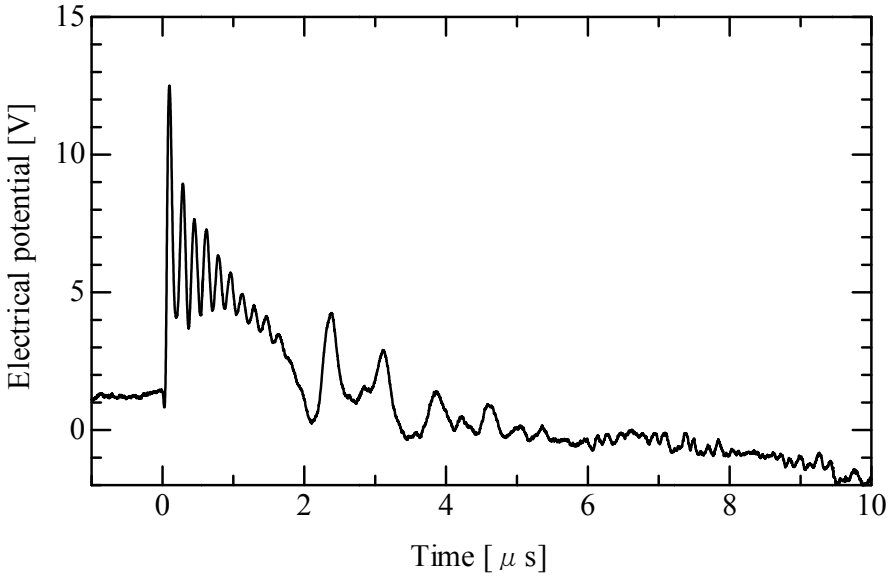

Fig. 12. Electrical potential measurement results.

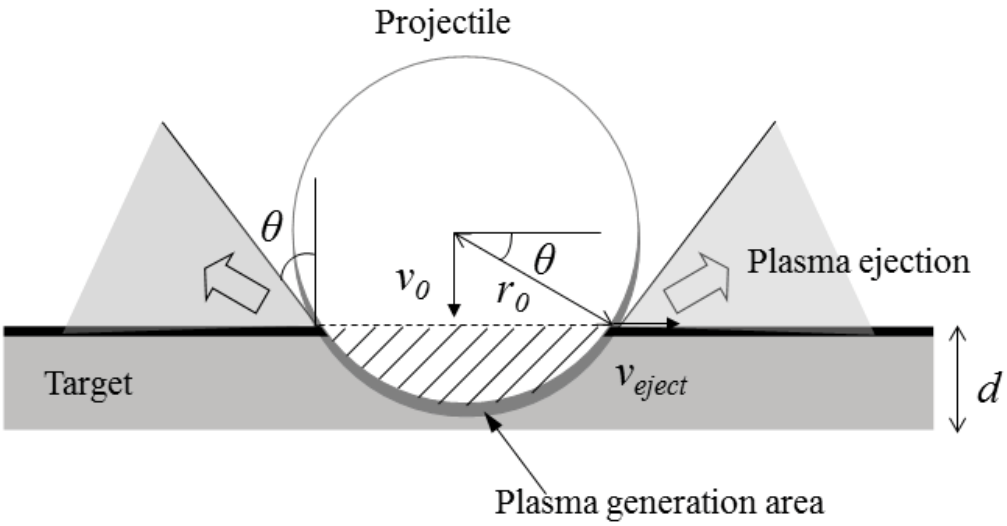

Fig. 13. Theoretical model. Perpendicular impact on the thin plate.

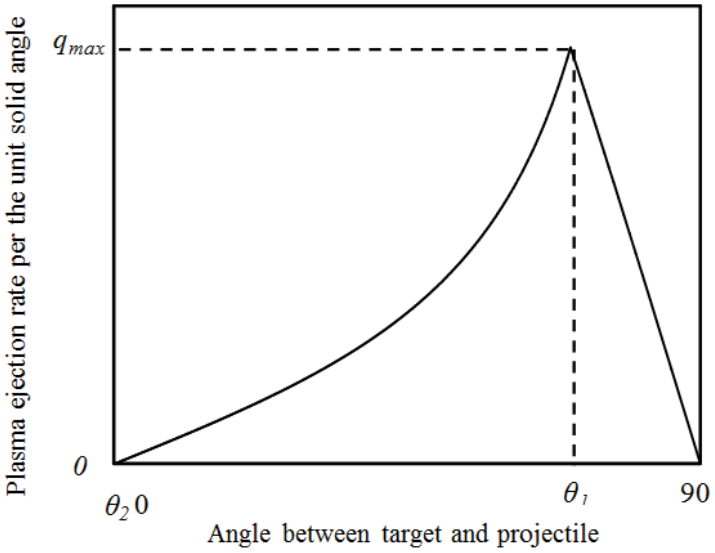

Fig. 14. Relation of plasma ejection rate to the θ angle.